D Cioranescu and J L Lions (Editors)
Centre National de la Recherche Scientifique/Collège de France

Nonlinear partial differential equations and their applications Collège de France Seminar VOLUME XIII

LONGMAN

Addison Wesley Longman Limited
Edinburgh Gate, Harlow
Essex CM20 2JE, England
and Associated Companies throughout the world.

Published in the United States of America
by Addison Wesley Longman Inc.

First published 1998

AMS Subject Classifications (Main) 35, 49, 93
(Subsidiary) 65, 73, 76

ISSN 0269-3674

ISBN 0 582 36926 6

Visit Addison Wesley Longman on the world wide web at
http://www.awl-he.com

British Library Cataloguing in Publication Data

A catalogue record for this book is
available from the British Library

Printed in Great Britain by Henry Ling Ltd.,
at the Dorset Press, Dorchester, Dorset.

Contents

[11] E. HRUSLOV: "The asymptotic behavior of solutions of the second boundary value problem under fragmentation of the boundary of the domain", Maths. USSR Sbornik, Vol. 35 (1979), No. 2.

[12] E. HRUSLOV - V. MARCHENKO: "Boundary-value problems in domains with fine-grained boundaries", Nauk. Dumka, Kiev (1974).

[13] L. MASCARENHAS - D. POLISEVSKI: "The warping, the torsion and the Neumann problems in a quasi-periodically perforated domain", M^2AN 28 (1) (1994) 37-57.

[14] N. G. MEYERS: "An L^p-estimate for the gradient of solutions of second order elliptic divergence equations", Ann. Sc. Norm. Sup. Pisa, 17 (1963), 189-206.

[15] F. MURAT: "H-Convergence", Séminaire d'Analyse Fonctionnelle et Numérique, 1977/1978, Univ. d'Alger, Multigraphed.

[16] S. SPAGNOLO: "Sulla convergenza di soluzioni di equazioni paraboliche ed ellittiche", Ann. Sc. Norm. Sup. Pisa 22 (1968), 571-597.

[17] L. TARTAR: "Cours Peccot au Collège de France", 1977.

[18] M.VANNINATHAN: "Homogenization of eigenvalue problems in perforated domains", Proc. Indian Acad. of Sciences 90 (1981), 239-271.

M. Briane: Département de Mathématiques (Université Paris 12) et Laboratoire d'Analyse Numérique, Université Pierre et Marie Curie, 4 Place Jussieu, 75230 Paris Cedex 05, France.

A. Damlamian: Département de Mathématiques (Université Paris 12) et Centre de Mathématiques, École Polytechnique, 91128 Palaiseau Cedex, France.

P. Donato: URA CNRS 1378 (Université de Rouen) et Laboratoire d'Analyse Numérique, Université Pierre et Marie Curie, 4 Place Jussieu, 75230 Paris Cedex 05, France.

E DELEERSNIJDER

Some mathematical problems in marine modelling

"Science is now a tripartite endeavour with Simulation added to the two classical components, Experiments and Theory" (Robinson, 1987). The routine use of numerical "simulation in scientific research (numerical experimentation, sensitivity and process studies, etc.) is thought by many to represent the first major step forward in the basic scientific method since the seventeenth century" (Robinson, 1987).

Marine sciences have, over the last decade, largely benefited from the advent of complex numerical models. Working out such models does however pose numerous mathematical problems.

For instance, the algorithm selected for solving the equations of the model must provide accurate results. To do so, the numerical scheme must be, at least, consistent and stable. Consistency is in general easily verified, while studying the stability of the numerical scheme may require a significant effort, sometimes giving rise to unpleasant surprises, as will be shown in Section 1 (see also Beckers and Deleersnijder, 1993).

Complex marine models routinely output millions, or even billions, of real numbers, the analysis and interpretation of which are far from straightforward. In fact, understanding such a large amount of information is a real challenge. Simple models may be helpful for interpreting the results of a complex one, as exemplified in Section 2 (see also Deleersnijder, 1994).

1. Numerical stability of inertia-gravity waves

Large scale atmospheric and oceanic motions roughly obey the geostrophic equilibrium. When imbalances occur, the geostrophic balance is restored by means of inertia-gravity waves (Blumen, 1972). The dynamics of tides and storm surges is dominated by the propagation of external inertia-gravity waves, which are related to the motion of the sea surface. In strongly stratified seas, one also considers the displacement of density surfaces, which leads to internal inertia-gravity waves. The propagation of inertia-gravity waves, be they external or internal, is thus a central issue to many geophysical fluid models. Hence, it is of the highest importance that the numerical scheme utilized be able to properly represent the propagation of those waves.

The external linear inertia-gravity waves, also called Poincaré waves, are governed by the following dimensionless equations:

$$\frac{\partial \eta}{\partial t} = -\frac{\partial u}{\partial x} - \frac{\partial v}{\partial y} , \tag{1}$$

$$\frac{\partial u}{\partial t} = \gamma v - \frac{\partial \eta}{\partial x} , \tag{2}$$

$$\frac{\partial v}{\partial t} = -\gamma u - \frac{\partial \eta}{\partial y} , \tag{3}$$

where t is time; u and v denote horizontal velocity components in the x and y direction, respectively; and η represents the sea surface elevation. The characteristic length, L, and time, T, used in the derivation of the dimensionless variables obey $L^2 = ghT^2$, where g is the gravitational acceleration and h is the unperturbed depth of the sea, assumed to be constant. The velocity scale, U, and the elevation scale, E, satisfy $E^2 = hU^2/g$. In addition, f being the Coriolis parameter, γ is defined to be $\gamma = fT$, so that the pure gravity waves correspond to $\gamma = 0$.

The governing equations of internal inertia-gravity waves are similar to (1)-(3), except that h, u, v and η are to be interpreted as equivalent quantities related to the particular internal mode considered (LeBlond and Mysak, 1978).

Various studies focused on the space differencing aspects of (1)-(3). When time differencing is also considered, it is customary to restrict the analysis to pure gravity waves ($\gamma = 0$), for which stability conditions are readily obtained. It is common to content oneself with the latter conditions. Here, on the example of a simple space-time differencing scheme, it is seen that the stability condition of the algorithm representing the propagation of inertia-gravity waves ($\gamma \neq 0$) is far more constraining than that of the pure gravity waves scheme. Indeed, the limit as $\gamma \rightarrow 0$ of the stability condition is not equal to the stability condition when $\gamma = 0$.

Numerical scheme. A forward-backward time stepping is selected (Mesinger and Arakawa, 1976). The Coriolis force is prevented from generating — or dissipating — mechanical energy by a simple technique stemming from Sielecki (1968) and adapted to ensure symmetry in the x and y directions. Centered space differencing is used, as in Arakawa and Lamb (1977). Accordingly, the discrete counterparts of (1)-(3) read

$$\eta^{n+1} = \eta^n - \Delta t \, (d_x u^n + d_y v^n) , \tag{4}$$

$$u^{n+1} = u^n - \Delta t \, [-\gamma s \, \overline{v}^{n+1} - \gamma (1-s) \, \overline{v}^n + d_x \eta^{n+1}] , \tag{5}$$

$$v^{n+1} = v^n - \Delta t \, [\gamma s \, \overline{u}^n + \gamma (1-s) \, \overline{u}^{n+1} + d_y \eta^{n+1}] , \tag{6}$$

where n is the index associated with the time discretization; Δt represents the dimensionless time increment; s is 0 or 1 according to whether n is even or odd; d_x and d_y denote the discrete space derivation operator along the x and y axis, respectively; the overbar refers to the space average that may be needed to evaluate v (u) at a grid node where u (v) is defined.

Stability analysis. Considering wave solutions of (4)-(6), the von Neumann stability analysis may be performed, leading to a 3x3 amplification matrix, the eigenvalues, λ, of which are given by

$$(\lambda - 1) \, (\lambda^2 - 2b\lambda + 1) = 0 . \tag{7}$$

As the time-independent geostrophic motion is a possible solution to (4)-(6), one eigenvalue must obviously be unity, in accordance with (7). Equations (1)-(3) contain no phenomenon growing in time, which implies that $|\lambda| \leq 1$ or, equivalently, $-1 \leq b \leq 1$.

Upon defining $\phi = \gamma \Delta t$ and $\xi = \xi_x + \xi_y$, b reads

$$b = 1 - 8 \frac{(\xi_* - \xi) \, \xi}{\xi_*^2} - 2\alpha^2 \phi^2 \left[\frac{4 \xi_x \xi_y}{\xi_*^2} + \frac{(\xi_* - 2\xi)}{\xi_*} \right] , \tag{8}$$

where α, ξ_x and ξ_y are positive functions of the wavenumbers (k_x, k_y) associated with the (x, y) coordinates, while ξ_* is a positive constant. The expression of α, ξ_x, ξ_y and ξ_* depends on the type of space grid considered, which may be A, B, C or D, according to Arakawa's classification (Arakawa and Lamb, 1977) (more details may be found in Beckers and Deleersnijder (1993)).

Putting $\phi = 0$ yields the well-known pure gravity waves problem, of which the necessary and sufficient stability condition is $\xi \leq \xi_*$. When $\phi \neq 0$, for $\xi \rightarrow \xi_*/2$, one has $b = -1 - 8 \, \alpha^2 \phi^2 \xi_x \xi_y / \xi_*^2$. It follows that numerical stability necessitates $\xi \leq \xi_*/2$. Therefore, the maximum admissible time step is, at most, equal to that of pure gravity waves divided by a factor of $\sqrt{2}$. This holds true whatever the value of γ, provided $\gamma \neq 0$!

As may be seen in (8), b is a quadratic function of ξ_x and ξ_y. That the stability constraint for $\phi = 0$ is different from that found for $\phi \rightarrow 0$ stems from a singular perturbation problem arising because ϕ^2 is a multiplicative factor of $\xi_x \xi_y$, which is one of the highest degree terms of (8). An illuminating graphical interpretation thereof may be achieved.

Graphical interpretation. Given a fixed value of b and α, (ξ_x, ξ_y) describes an elliptical path in the (ξ_x, ξ_y) space. By varying b one obtains concentric ellipses whose axes grow as b increases. The minor axis of these ellipses lies on the symmetry axis $\xi_x = \xi_y$.

According to the stability criterion $-1 \leq b \leq 1$, the subspace $\xi_x, \xi_y \geq 0$ is divided into three areas, A_-, $A_0 = A_{0,1} \cup A_{0,2}$, and A_+, corresponding to $b < -1$, $-1 \leq b \leq 1$, and $1 < b$ (Fig. 1). The stability conditions must be such that (ξ_x, ξ_y) always lies in A_0. Since ξ_x and

ξ_y may vary — not necessarily independently — from 0 to their respective maxima, it is clear that (ξ_x, ξ_y) cannot enter $A_{0,2}$ without crossing A_-. Hence, the actual stability constraint must force (ξ_x, ξ_y) to remain within $A_{0,1}$. When $\phi = 0$, the $b = -1$ ellipse limiting A_- transforms to a straight line so that A_- vanishes: the stability area is then A_0, instead of $A_{0,1}$ only. This "jump" of the stability domain explains easily the fact that the stability condition changes with a discontinuity when switching from $\gamma = 0$ to $\gamma \neq 0$.

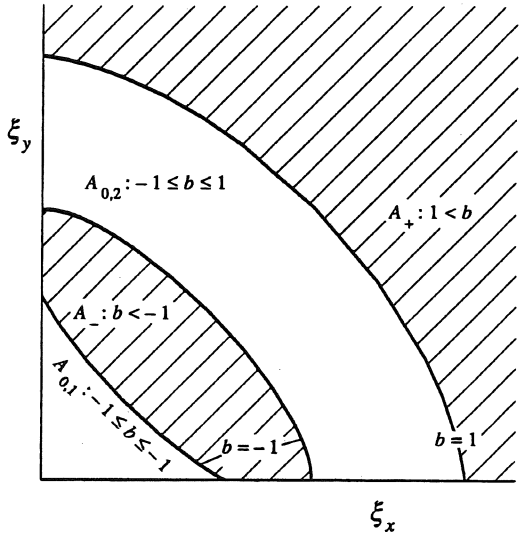

Figure 1. Stability and instability (hatched) regions for $0 < \phi^2 \le 1$ and $0 < \alpha$.

C-grid stability criteria. For the C-grid, which is used in many marine models, $\alpha = |\cos\theta_x \cos\theta_y|$, $\xi_* = 1$, $\xi_x = (\Delta t / \Delta x)^2 \sin^2\theta_x$ and $\xi_y = (\Delta t / \Delta y)^2 \sin^2\theta_y$ — with $0 \le 2\theta_x = k_x \Delta x \le \pi$ and $0 \le 2\theta_y = k_y \Delta y \le \pi$, Δx and Δy being the dimensionless space increments. It may then be shown that the necessary and sufficient stability conditions are

$$\Delta t \le \frac{\Delta x \, \Delta y}{(\Delta x^2 + \Delta y^2)^{1/2}} \tag{9}$$

for pure gravity waves ($\phi = 0$), and

$$|\phi| \le 1 \quad \text{and} \quad \Delta t \le \frac{1}{\sqrt{2}} \frac{\Delta x \, \Delta y}{(\Delta x^2 + \Delta y^2)^{1/2}} \tag{10}$$

for inertia-gravity waves ($\phi \neq 0$). As expected, condition (10) is more restrictive than (9).

Conclusion. The example above provides a striking illustration of the fact that studying a too simple subset of equations may lead to inappropriate stability criteria. This topic has rarely been addressed, probably because of the difficulty of the relevant mathematical manipulations. Among those who have however dealt with similar problems, it is worth putting forward the work of Cushman-Roisin (1984), who has obtained very interesting results.

2. Interpretation of three-dimensional model results

We now turn our attention to the problem of interpreting the large amount of information generated by marine models.

Most quantities computed by marine models are four-dimensional, *i.e.*, they depend on time and three space coordinates. Since the vast majority of the graphical tools are two- or three-dimensional, the graphical representation of the model results requires appropriate mapping onto a two- or three-dimensional space. This may be carried out in numerous ways by means of existing graphical packages.

One must however bear in mind that the role of computer graphics is not just to produce attractive pictures, but to help gain insight into the physics of the marine flow under study. In other words, physical intuition and reasoning are also needed if profound understanding of the flow's mechanisms is sought. Schematically, this may be expressed by the following relation: quality of the interpretation = (physical skill) x (computer graphics skill). This implies, for instance, that the best graphical software will probably prove useless if operated by someone having no idea of ocean dynamics!

An example of an interpretation method based on little graphical skill but considerable physical skill is given in the study of the vertical velocity field produced by the Liège University hydrodynamic model applied to the region of the Bering Strait (Deleersnijder, 1994).

All variables that will be analysed below are obtained from a steady state solution. As a consequence, they are only three-dimensional.

Eco-hydrodynamics of the Bering Strait region. The Pacific and Arctic Oceans exchange mass, momentum and energy through the Bering Strait only. The region of the Bering Strait exhibits some of the most intense biological productivity ever measured in the sea (Sambrotto *et al.*, 1984). From a physical and biological point of view, this region is thus of high importance.

The hydrodynamic model study — extensively discussed in Deleersnijder (1992), Nihoul *et al.* (1993) and Deleersnjder (1994) — was carried out in an ecological perspective and concentrated on the summer period, when the region of interest is virtually free of sea

ice. The computational domain was a 700 km x 700 km shallow sea area, where the sea depth is $\lesssim$ 70 m (Fig. 2).

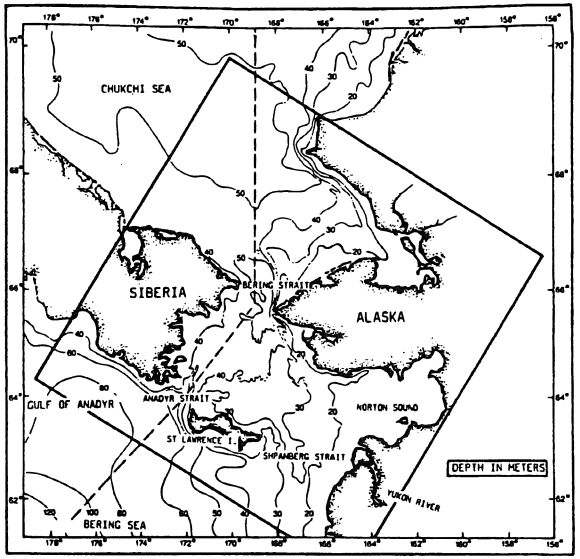

Figure 2. Limits of the computational domain, with bathymetry (depth in meters).

Since the ultimate aim of the study was the understanding of the biological activity, it was deemed appropriate to devote most of the attention to the general circulation, *i.e.*, the flow averaged over a sufficiently long time, say one week to one month, so that the meso-scale processes are filtered out. In the domain of interest, the general circulation is associated with much of the kinetic energy, in marked contrast to what is observed in most shelf seas.

The monthly flow through the Bering Strait is directed to the North, *i.e.*, from the Pacific to the Arctic. Since Coachman and Aagaard (1966), it seems clear that this northward flow is primarily induced by the water level difference between the Pacific and the Arctic. It is also believed that the variability of the flow mainly results from the wind forcing (Coachman and Aagaard, 1988). On average, two thirds of the flow pass through the Anadyr Strait.

In the domain of interest the salinity variations are predominantly horizontal, whereas the temperature contrasts are mostly observed in the vertical direction, with a marked thermocline (Coachman *et al.*, 1975). Satellite infra-red pictures show that a plume of cold

water originates in the Anadyr Strait, near the Siberian coast. Although its extent depends on meso-scale phenomena, the cold water plume seems to be a permanent hydrodynamic feature (Fig. 3).

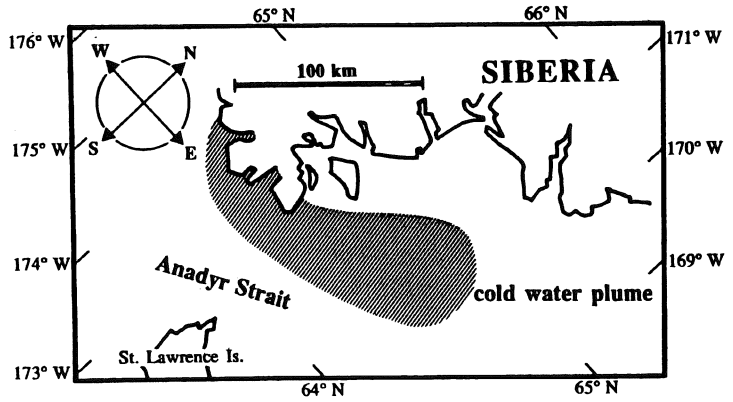

Figure 3. Schematic representation of the plume of cold water downstream of the Anadyr Strait.

All *in situ* data analysed by Brasseur (1991) and Brasseur and Haus (1991) confirm the existence and persistence of a plume of cold water downstream of the Anadyr Strait and suggest that it is due to an intense upwelling taking place in the "Siberian half" of Anadyr Strait. Throughout the summer period the Anadyr upwelling is likely to bring nutrients from the lower layer to the euphotic zone, continuously fueling the primary production (Walsh *et al.*, 1989).

Model set-up. No device is able to directly measure vertical fluxes at reasonable cost. Moreover, indirect methods for estimating the magnitude of the vertical motions are known not to be very accurate. This pointed to the need for a three-dimensional hydrodynamic model to compute the vertical fluxes in the domain of interest.

The main objective of the hydrodynamic model study was thus the evaluation of the vertical fluxes, to test the hypothesis that it is mainly the Anadyr stream which is fueling the huge biological production of the Northern Bering Sea.

The model set-up was described in detail by Deleersnijder (1994). Here it is sufficient to say that the water was forced to enter the domain through the southern boundary and that no wind stress was applied. Three reasons led to neglecting the wind forcing. First, the intent was to simulate the steady state background flow, *i.e.*, the circulation free of wind-induced variability. Second, it was believed that the wind stress is not a major forcing in the domain of interest, although, over the whole Bering-Chukchi shelf, the wind stress certainly plays a major role. Third, the plume of cold water downstream of the Anadyr Strait does not seem

to obey the classical wind-induced coastal upwelling scenario. Wind data indeed indicates that the wind stress is hardly ever directed so as to drive coastal upwelling (Deleersnijder, 1992). Therefore, it was found appropriate to look for an upwelling mechanism in which the wind stress has no significant role.

Sigma-coordinate. The equations of the model are solved numerically in the sigma-coordinate system (Phillips, 1957). Accordingly, the vertical coordinate z — increasing upwards — is transformed to

$$\sigma = \frac{z + h}{\eta + h} , \tag{11}$$

where h and η denote, as in the preceding section, the unperturbed sea depth and the sea surface elevation, respectively. Hence, the actual height of a water column is $H = h + \eta$. In the sigma-coordinate system, the surface ($z = \eta$) and the bottom ($z = -h$) of the sea are coordinate surfaces. The latter is defined as $\sigma = 0$, while the former corresponds to $\sigma = 1$.

Along with (11), it is customary to use a new vertical velocity, defined as $D_t \sigma$, where D_t represents the material derivative operator. With the transformed vertical velocity, the impermeability of the surface and the bottom is easily taken into account by $D_t \sigma = 0$ at $\sigma = 1, 0$.

In the sigma-coordinate system, the equations of the model do not explicitly involve the "physical" vertical velocity w. Computing the latter is then part of the postprocessing of the model results.

Upsloping and upwelling. As suggested by Waleffe (1985) and Deleersnjder (1989), it is useful to split w into two contributions, *i.e.*, $w = w_{US} + w_{UW}$.

For a time-independent flow, the upsloping velocity w_{US} reads

$$w_{US} = -\mathbf{u} \bullet [\, (1 - \sigma) \nabla h - \sigma \nabla \eta \,] , \tag{12}$$

where $\mathbf{u}$ is the horizontal velocity vector and ∇ denotes the horizontal "gradient operator". It may be seen that a particle moving with a velocity equal to $\mathbf{u} + w_{US}\mathbf{e}_z$ — where $\mathbf{e}_z$ is the vertical unit vector — does not cross any iso-σ surface, implying that this particle remains at the same relative height in the water column. Since the bottom and the surface are iso-σ surface, w_{US} may be regarded as the vertical velocity adapted to the slope of the surface and the bottom.

The upwelling velocity,

$$w_{UW} = H D_t \sigma , \tag{13}$$

is the velocity with which the water crosses the iso-σ surfaces. Therefore, w_{UW} may be interpreted as the vertical velocity associated with "true" up- or down-welling motions.

This decompositon of the vertical velocity provides an interesting analysis tool, since it renders it possible to distinguish between the part of the vertical velocity that is necessary for the flow to accommodate to the geometry of the basin and the extra vertical velocity related to actual up- or down-wellings.

A significant drawback must nevertheless be highlighted. Definitions (12) and (13) are purely arbitrary: it is indeed possible to put forward several alternative expressions of w_{US} and w_{UW} that could be equally valid as regards the distinction between the vertical motions that are associated with the geometry of the basin and those that are not. What justifies (12) and (13) is only that they take advantage in a very natural way of the use of the sigma coordinate system. In a certain sense, (12) and (13) are inherent in the sigma-transformation.

In accordance with the present reasoning, we will examine separately the upsloping and upwelling velocities.

Upsloping velocity field. To understand the space distribution of the upsloping velocity, it is desirable to identify the dominant terms of definition (12). The sea surface elevation does not exceed ± 0.4 m (Deleersnijder, 1992). Hence, in (12), $\sigma \nabla \eta$ may be neglected compared with $(1 - \sigma) \nabla h$. Let $\hat{\mathbf{u}} = \mathbf{u} - \bar{\mathbf{u}}$ denote the deviation of the horizontal velocity relative to its depth-average $\bar{\mathbf{u}}$ (Fig. 4). Model results indicate that, roughly speaking, $|\hat{\mathbf{u}}| \approx 0.1\ |\bar{\mathbf{u}}|$ (Deleersnijder, 1992). It is thus suggested approximating w_{US} by a "simplified upsloping velocity" defined as $w_{US,S} = -(1 - \sigma)\, \bar{\mathbf{u}} \bullet \nabla H$, which may be transformed to an expression better suited to numerical calculations, *viz* $w_{US,S} = (1 - \sigma)\, H\, \nabla \bullet \bar{\mathbf{u}}$.

The simplified upsloping velocity turns out to be reasonably close to w_{US}. Indeed, upon denoting $|s|_{rms}$ the root mean square taken over the whole computational domain of a variable s, one has $|w_{US,S} - w_{US}|_{rms} / |w_{US}|_{rms} = 0.24$, which means that $w_{US,S}$, roughly speaking, accounts for 76% of w_{US}.

The most advantageous feature of the simplified upsloping velocity is that, over each water column, the values of $w_{US,S}$ are self-similar: $|w_{US,S} / (H \nabla \bullet \bar{\mathbf{u}})|$ is a linear function of σ only, which is zero at the surface and maximum at the bottom.

Since w_{US} is close to $w_{US,S}$, the vertical profiles of the upsloping velocity are nearly self-similar. As a result, to interpret the three-dimensional field of upsloping velocity, it is sufficient to display a depth-independent quantity such as, for instance, the depth-mean upsloping velocity $\bar{w}_{US}$ (Fig. 5). It would be less appropriate to simply display the upsloping velocity in a series of horizontal planes of section located at various depths below the surface. Doing that would result in confusing pictures in which it would be difficult to distinguish between the horizontal variablity of w_{US} that is intrinsic to the flow and that associated with the plane of section being, from one location to another, relatively closer or more distant to the sea surface or bottom.

Looking simultaneously at Figs. 2, 4 and 5, one immediately notices that, as expected, the upsloping velocity is positive where the flow is directed towards shallower regions and is negative otherwise. Furthermore, $|\bar{w}_{US}|$ is maximum in the vicinity of Anadyr and Bering Straits, *i.e.*, in the regions where the horizontal current most clearly crosses the isobaths while having a large speed. In particular, the upsloping velocity is high in the Anadyr Strait, indicating significant upwards water fluxes.

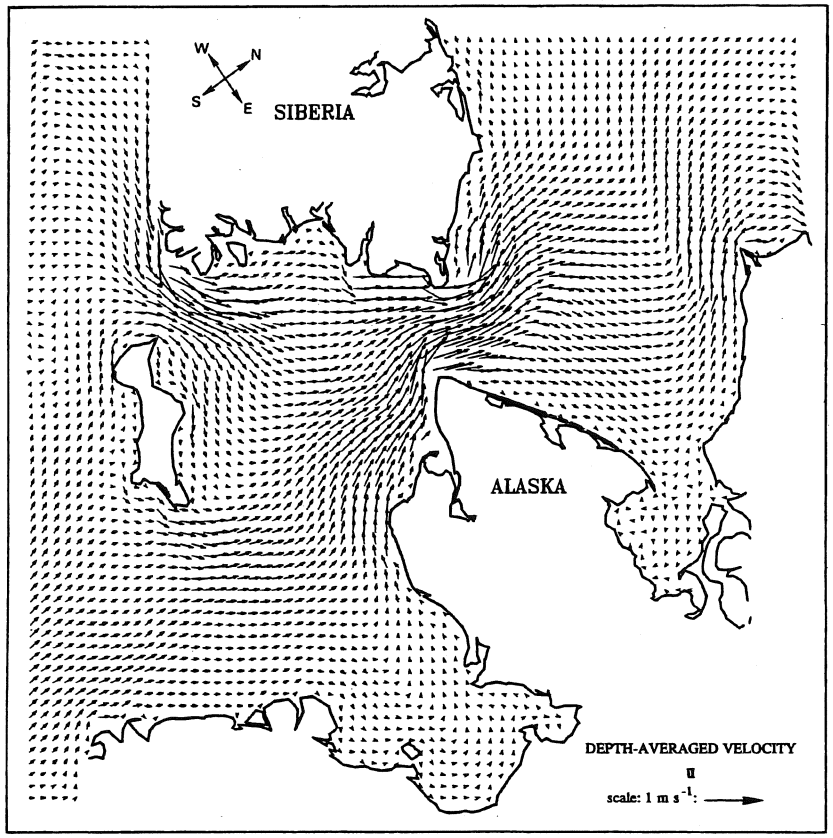

Figure 4. Depth-averaged horizontal velocity field computed by the model.

It must be pointed out that the upsloping velocity cannot bring a water parcel up to the surface. However, when the upsloping velocity is positive, every water parcel comes closer to the surface, while remaining at the same relative height in the water column. This may render it more likely for the turbulent diffusion to mix some of the water column, or even the whole water column, since the height of fluid to be mixed decreases. Whether or not this hypothesis is correct is difficult to verify, because this mechanism involves two processes interacting non-linearly. Anyway, this process, if it actually exists, could be responsible for part of the cold water plume developing downstream of the Anadyr Strait.

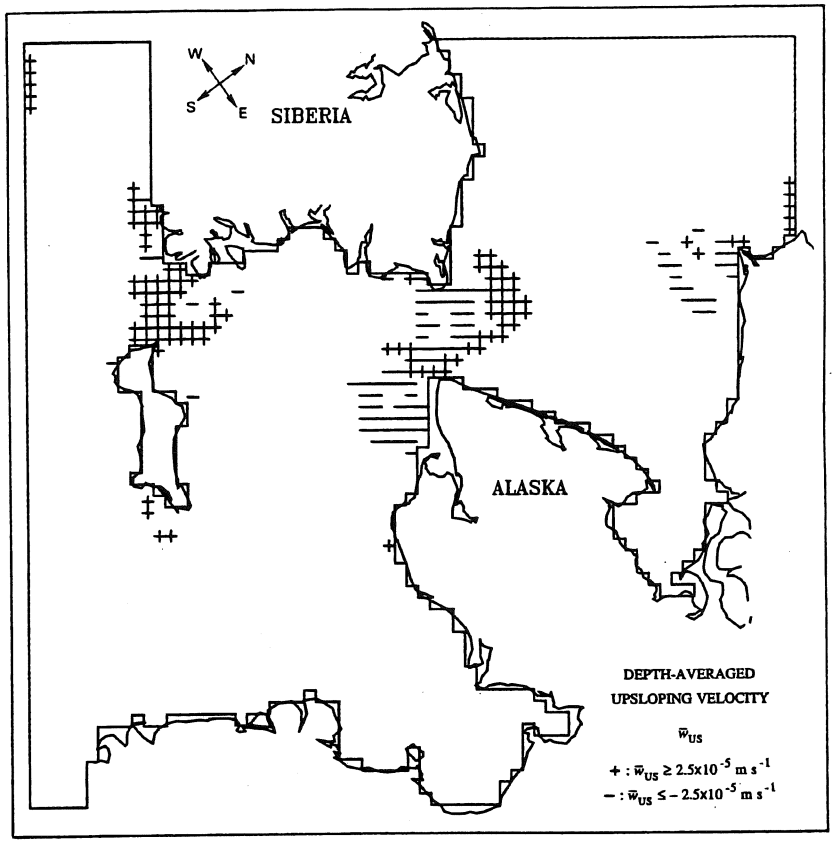

Figure 5. Depth-averaged upsloping velocity.

Upwelling velocity field. According to the model results (Deleersnijder, 1992), most vertical profiles of w_{UW} are of the same type: as σ increases from 0 to 1, $|w_{UW}|$ grows from zero at the bottom, reaches a maximum and finally decreases to zero at the surface. However, the location of the maximum of $|w_{UW}|$ may vary very widely from one vertical to

another. Although the vertical profiles of w_{UW} are not close to being self-similar, they exhibit enough common features for a method resembling that used to display w_{US} to be feasible for the graphical representation of the field of upwelling velocity (Fig. 6).

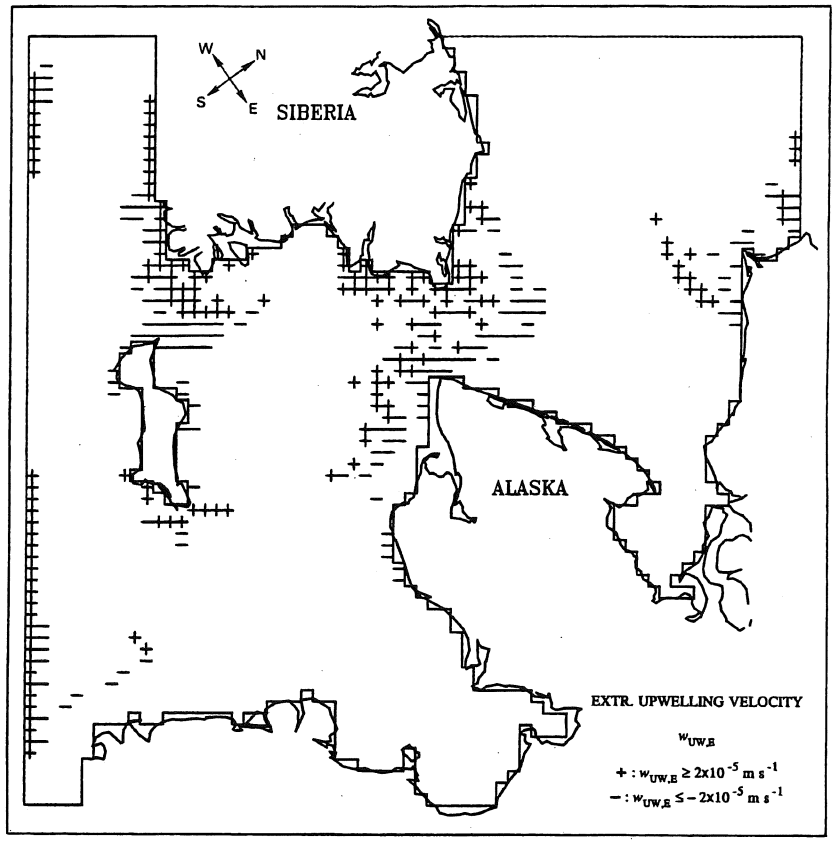

Figure 6. Representation of the upwelling velocity. For each water column, one takes into account the extremum of the upwelling velocity, $w_{UW,E}$, *i.e.*, the value of w_{UW} that has the maximum absolute value.

Significant up- and down-wellings are found in small areas. Upwelling phenomena taking place in the one grid box wide strip along the southern open boundary clearly correspond to an artefact due to improper boundary conditions imposed on the horizontal velocity (Deleersnijder, 1992). In the region of the Anadyr Strait, close to the Siberian coast, the upwelling velocity is directed upwards and can be as high as 10 m day^{-1}. Thus, the upwelling velocity is large enough to bring the thermocline, initially located at $z = -15$ m, up to the surface.

An upwelling mechanism. As previously stated, the wind forcing is not the main cause of the vertical motions. It follows that one has to look for another upwelling mechanism. Inspiration can be found in the Ekman pumping theory set out in classical treatises of geophysical fluid mechanics (*e.g.*, Cushman-Roisin, 1994).

It may be seen that

$$w_{UW} = -\int_0^\sigma \tilde{\nabla}\bullet(H\,\hat{\mathbf{u}})\;\mathrm{d}\sigma\;, \tag{14}$$

where $\tilde{\nabla}$ denotes the sigma-space counterpart of ∇. Consequently one has to analyse the behaviour of $H\hat{\mathbf{u}}$ in order to understand the distribution of w_{UW}.

The direction of $\mathbf{u}$ with respect to $\bar{\mathbf{u}}$ is measured by the angle β, which may be calculated from $\sin\beta = \mathbf{e}_z\bullet(\bar{\mathbf{u}}\times\mathbf{u}) / (|\bar{\mathbf{u}}|\,|\mathbf{u}|)$. Angle β is positive if $\mathbf{u}$ is "on the left of $\bar{\mathbf{u}}$", and is negative otherwise. For each water column, the veering Ξ is defined as $\Xi = \beta_{max} - \beta_{min}$, if the point where $\beta = \beta_{max}$ is closer to the bottom than that where $\beta = \beta_{min}$. Otherwise, $\Xi = \beta_{min} - \beta_{max}$. The mean veering is about 12°. The veering is positive in 2556 verticals out of a total of 2690. In other words, in 95% of the verticals of the computational domain, the direction of $\mathbf{u}$ is qualitatively in agreement with that of the bottom Ekman spiral, *i.e.*, $\mathbf{u}$ is on the left of $\bar{\mathbf{u}}$ near the bottom and on the right near the surface. This is not surprising, since it may shown that, in the present case, the Ekman momentum equations encompass the dominant terms of the horizontal momentum equations (Deleersnijder, 1992).

The qualitative properties of $H\hat{\mathbf{u}}$ are accounted for in the following Taylor expansion of $H\hat{\mathbf{u}}$ truncated at two terms:

$$H\,\hat{\mathbf{u}} = (H\,\hat{\mathbf{u}})_{/\!/} + (H\,\hat{\mathbf{u}})_{\perp}\;, \tag{15}$$

with

$$[(H\,\hat{\mathbf{u}})_{/\!/}, (H\,\hat{\mathbf{u}})_{\perp}] = (1-2\sigma)\,[-a_{/\!/}, a_{\perp}\,\mathbf{e}_z\mathbf{x}]\,H\bar{\mathbf{u}}\;, \tag{16}$$

where $a_{/\!/}$ and $a_{\perp}$ are positive constants. Relations (15) and (16) are by no means intended to provide a reliable approximation to the vertical profiles of $H\hat{\mathbf{u}}$. Instead, (15)-(6) are simply caricatured formulae having some of the modelled properties of $H\hat{\mathbf{u}}$: in (15)-(16), the depth average of $|\hat{\mathbf{u}}|$ is a linearly increasing function of $|\bar{\mathbf{u}}|$, and the veering is always positive. Combining (14)-(16) yields $w_{UW} = a_{\perp}\,\mathbf{e}_z\bullet(\nabla\times H\bar{\mathbf{u}})\;\sigma(1-\sigma)$, implying

$$\text{sign}(\bar{w}_{UW}) = \text{sign}[\mathbf{e}_z \bullet (\nabla \times H\bar{\mathbf{u}})] \ , \qquad (17)$$

where $\bar{w}_{UW}$ represents the depth-average of the upwelling velocity.

Whether or not the sign of the upwelling velocity is actually given by the sign of the curl of the transport $H\bar{\mathbf{u}}$ is easily checked. It turns out that (17) provides an excellent account of the model results (Table 1).

Table 1. Assessment of (17): n_+ denotes the number of water columns where the sign of the depth-averaged upwelling velocity is equal to that of $\mathbf{e}_z \bullet (\nabla \times H\bar{\mathbf{u}})$, while n_- is the number of verticals where (17) does not apply; $\bar{w}_{UW}$ is expressed in 10^{-5} m s^{-1}.

	n_+	n_-	$\frac{n_+}{n_+ + n_-}$
$\lvert\bar{w}_{UW}\rvert \geq 0.1$	1547	315	0.83
$\lvert\bar{w}_{UW}\rvert \geq 1$	240	69	0.78
$\lvert\bar{w}_{UW}\rvert \geq 3$	30	3	0.91
$\lvert\bar{w}_{UW}\rvert \geq 5$	10	1	0.91
$\lvert\bar{w}_{UW}\rvert \geq 7$	1	0	1.00
$\lvert\bar{w}_{UW}\rvert \geq 9$	0	0	

The mechanism of the up- and down-wellings is thus as follows. The main driving force of the horizontal velocity is the part of the pressure force that is associated with the gradient of the sea surface elevation. Due to frictional forces associated with the bottom stress, the horizontal velocity is not identically equal to its depth-average. Moreover, the Coriolis force induces a positive veering of the velocity. The resulting space variations of $(H\hat{\mathbf{u}})_\perp$, correlated with those of $H\bar{\mathbf{u}}$, lead to local divergence or convergence of $H\hat{\mathbf{u}}$, implying vertical motion in the sigma-space. The variations of $(H\hat{\mathbf{u}})_{//}$ should have no impact on the upwelling velocity, which is reasonably well confirmed by the model results (Deleersnijder, 1992).

What has been done above simply amounts to adapting the Ekman pumping theory to our results, where the bottom stress turns out to be the ultimate cause of the vertical motions.

Conclusion. Synthetic information has been extracted from the 26,900 values of the transformed vertical velocity computed by the model. The analysis technique, based on the splitting of the vertical velocity into two components, has been shown to work rather well for two main reasons. First, upsloping and upwelling are very different processes. Second, the typical profiles of the corresponding vertical velocities are completely dissimilar.

The vertical velocity field produced by the model in the vicinity of the Anadyr Strait is qualitatively in agreement with the observations. According to the results of the model, the Anadyr Strait plume of cold water is due to an upwelling process, possibly combined with upsloping and turbulent diffusion. The upwelling mechanism identified in the simulated currents closely resembles the classical Ekman pumping process, which is a concept generally used in deep seas. It is proposed that the notion of shallow-sea Ekman pumping be introduced, as a process concerning the whole water column.

The velocity field discussed above has been used as an input to an ecological model, confirming the crucial role of the Anadyr Strait upwelling in fueling the primary production (Adam, 1990; Nihoul *et al.*, 1993).

References

Adam, P. (1990) *Modélisation Mathématique Tridimensionnelle d'un Ecosystème Marin – Application à la Région du Détroit de Bering*, Mémoire de Fin d'Etudes, Faculté des Sciences Appliquées, Université de Liège, 159 pp.

Arakawa, A. and Lamb, V.R. (1977) Computational design of the basic dynamical processes of the UCLA general circulation model, *Methods in Computational Physics*, Vol. 17, Academic Press, 337 pp.

Beckers, J.-M. and Deleersnijder, E. (1993) Stability of a FBTCS scheme applied to the propagation of shallow-water inertia-gravity waves on various space grids, *J. Comput. Phys.*, 108, 95–104.

Blumen, W. (1972) Geostrophic adjustment, *Rev. Geophys. and Space Phys.*, 10, 485–528.

Brasseur, P.P. (1991) A variational inverse method for the reconstruction of general circulation fields in the Northern Bering Sea, *J. Geophys. Res.*, 96, 4891–4907.

Brasseur, P.P. and Haus, J. (1991) Application of a 3-D variational inverse model to the analysis of ecohydrodynamic data in the Northern Bering and Southern Chukchi seas, *J. Mar. Syst.*, 1, 383–401.

Coachman, L.K. and Aagaard, K (1966) On the water exchange through Bering Strait, *Limnol. Oceanogr.*, 11, 44–59.

Coachman, L.K. and Aagaard, K (1988) Transports through Bering Strait: annual and interannual variability, *J. Geophys. Res.*, 93, 15535–15539.

Coachman, L.K., Aagaard, K. and Tripp, R.B. (1975) *Bering Strait – The Regional Physical Oceanography*, Univ. of Washington Press, 172 pp.

Cushman-Roisin, B. (1984) Analytical, linear stability criteria for the leap-frog, Dufort-Frankel method, *J. Comput. Phys.*, 53, 227–239.

Cushman-Roisin, B. (1994) *Introduction to Geophysical Fluid Dynamics,* Prentice Hall, 320 pp.

Deleersnijder, E. (1989) Upwelling and upsloping in three-dimensional marine models, *Appl. Math. Model.,* 13, 462–467.

Deleersnijder, E. (1992) *Modélisation Hydrodynamique Tridimensionnelle de la Circulation Générale Estivale de la Région du Détroit de Bering*, Thèse de Doctorat, Faculté des Sciences Appliquées, Université Catholique de Louvain, 189 pp.

Deleersnijder, E. (1994) An analysis of the vertical velocity field computed by a three-dimensional model in the region of the Bering Strait, *Tellus,* 46A, 134–148.

Mesinger, F. and Arakawa, A. (1976) Numerical methods used in atmospheric models, *GARP Publications Series* (no. 17, vol. 1), WMO-ICSU Joint Organizing Committee, 64 pp.

LeBlond, P.H. and Mysak, L.A. (1978) *Waves in the Ocean,* Elsevier, 602 pp.

Nihoul, J.C.J., Adam, P., Brasseur, P., Deleersnijder, E., Djenidi, S. and Haus, J. (1993) Three-dimensional general circulation model of the northern Bering Sea's summer ecohydrodynamics, *Cont. Shelf Res.,* 13, 509–542.

Nihoul, J.C.J., Adam, P., Djenidi, S. and Deleersnijder, E. (1993) Modelling the coastal ocean's complex ecohydrodynamics – A case study: the Northern Bering Sea, *Progress in Belgian Oceanographic Research,* Royal Academy of Belgium, pp. 203–216.

Phillips, N.A. (1957) A coordinate system having some special advantages for numerical forecasting, *J. Meteorol.,* 14, 184–185.

Robinson, A.R. (1987) Predicting open ocean currents, fronts and eddies, *Three-Dimensional Models of Marine and Estuarine Dynamics* (J.C.J. Nihoul and B.M. Jamart, Editors), Elsevier, pp. 89–111.

Sambrotto, R.N., Goering, J.J. and McRoy, C.P. (1984) Large yearly production of phytoplankton in the Western Bering Strait, *Science,* 225, 1147–1150.

Sielecki, A. (1968) An energy-conserving difference scheme for the storm surge equations, *Mon. Weather Rev.,* 96, 150–156.

Waleffe, F. (1985) *Modèle Mathématique 3D de la Mer de Bering*, Mémoire de Fin d'Etudes, Faculté des Sciences Appliquées, Université de Liège, 126 pp.

Walsh, J.J., McRoy, C.P., Coachman, L.K., Goering, J.J., Nihoul, J.C.J., Whitledge, T.E., Blackburn, T.H., Parker, P.L., Wirck, C.D., Shuert, P.G., Grebmeier, J.M., Springer, A.M., Tripp, R.B., Hansell, D.A., Djenidi, S., Deleersnijder, E., Henriksen, K., Lund, B.A., Andersen, P., Müller-Karger, F.E. and Dean, K. (1989) Carbon and nitrogen cycling within the Bering/Chukchi Seas: source regions for organic matter affecting AOU demands of the Arctic Ocean, *Progr. Oceanogr.*, 22, 279-361.

Eric DELEERSNIJDER, Chercheur qualifié du F.N.R.S.
Institut d'Astronomie et de Géophysique G. Lemaître, Université Catholique de Louvain,
2 Chemin du Cyclotron, B–1348 Louvain-la-Neuve, Belgium. e-mail: ericd@astr.ucl.ac.be

J DESCLOUX, M FLUECK AND M V ROMERIO

A modelling of the stability of aluminium electrolysis cells

1 Introduction

In 1886, Hall and Héroult invented simultaneously the same procedure for producing aluminium; it is based on the electrolysis of alumina and remains in use all over the world. The increasing costs of energy oblige today the companies to persue their endeavours in order to improve the efficiency of their plants. One constitutive part of the global optimisation problem consists in insuring the stability of the motion of the fluids contained in the cells; this is the subject of this paper.

In Section 2, we give a description of a cell and present the basic time dependent magnetohydrodynamic equations that we shall adopt for describing the phenomena which are relevant to the stability problem.

For defining the notion of stability, we use the simplest approach which is the linear one. In Section 3, we establish with some details the equations of the linear stability modelling. We give of these ones variational formulations which are more suitable for computational purposes and sketch some numerical algorithms; this is the content of Section 4.

Section 5 concludes the paper with some comments and numerical results.

In this study, we insist on the modelling aspects of the problem. Although we sometimes use for convenience the mathematical language, we don't give any rigorous proof. Note however that Reference [2] contains some justifications of the modelling based on the spectral theory of linear operators.

The project on which we report here realizes to our knowledge the first attempt of a genuine tridimensional simulation of the stability of aluminium electrolysis cells and it requires the resources of the most recent computers. Some improvements may possibly be achieved for details. At present time it is however too early for judging the validity of the fundamental hypothesis of linear stability.

Among the different approaches found in the literature, let us quote the following ones : study of dispersion relations in Fourier analysis of linear models [3], [4], shallow water modelling [5], [6], numerical simulation of the dynamic MHD equations [4], [7], physical simulation in laboratories [4]. We furthermore mention the theoretical work [8] which establishes the stability of a two-dimensional modelling.

This work is supported by the Swiss CERS Foundation and ALUSUISSE-LONZA-SERVICES Ltd.